Research Article

Xuemei Zhang, Peng Zhang*, Weisuo Yuan, and Shaowei Hu

Durability prediction of geopolymer mortar reinforced with nanoparticles and PVA fiber using particle swarm optimized BP neural network

https://doi.org/10.1515/ntrev-2023-0214
received December 17, 2023; accepted February 5, 2024

Abstract: In this study, polyvinyl alcohol (PVA) fibers and nanoparticles were incorporated to enhance the durability of geopolymer mortar (GM) with metakaolin (MK) and fly ash (FA). The dosage of nano-SiO_2 (NS) was 0–2.5% and that of PVA fiber was 0–1.2%. The durability of GM includes resistance to chloride ion penetration, freeze–thaw cycles, and sulfate erosion. Compared with the single BP neural network (BPNN) model, a particle swarm optimized BPNN (PSO-BPNN) model was utilized to predict the resistance to chloride ion penetration, freeze–thaw cycles, and sulfate erosion of GMs with different dosages of nanoparticles and PVA fibers. In the model, the dosage of NS, PVA fiber, FA, and MK were used as input layers, and the durability parameters of electric flux, mass loss, and compressive strength loss of GMs were used as output layers. The result exhibits that the root mean square errors (RMSEs) of BPNN for resistance to chloride ion penetration, freeze–thaw cycles, and sulfate erosion of GM mixed with nanoparticles and PVA fibers are 145.39, 6.43, and 2.19, whereas RMSEs obtained from PSO-BPNN are 76.33, 2.87, and 1.03, respectively. The NN optimized by particle swarm algorithm has better prediction accuracy. The PSO-BPNN can be utilized for estimating durability of GM reinforced by NS and PVA fiber, which can provide a guide for the proportion design of GM with PVA fiber and NS as well as for the engineering practice in the future.

Keywords: geopolymer mortar, PSO-BP neural network, durability, prediction

*** Corresponding author: Peng Zhang**, School of Water Conservancy and Transportation, Zhengzhou University, Zhengzhou 450001, China, e-mail: zhangpeng@zzu.edu.cn
Xuemei Zhang, **Weisuo Yuan**, **Shaowei Hu:** School of Water Conservancy and Transportation, Zhengzhou University, Zhengzhou 450001, China

1 Introduction

As the economy develops by leaps and bounds, it is necessary to implement a large number of construction projects throughout the world. This requires that the technology of construction industry accelerates its development towards high efficiency, high performance, and sustainable development [1]. As one of the most important materials in the construction of building projects, cementitious materials are essential for the production of concrete [2]. Currently, the most widely used cementitious material in the world is silicate cement [3,4]. Cement not only consumes huge energy in the production process but also releases a large amount of greenhouse gas CO_2 [5–7]. According to incomplete statistics, an estimated 1.35 billion tons of CO_2 are released annually by the cement industry worldwide, making up 7% of total anthropogenic carbon emissions. In recent years, with the continuous growth of the world population, the demand for housing has followed the rapid rise, and the demand for cement in the construction industry has also shown a linear upward trend. Against this background, there is a more difficult time in environmental management all over the world, with the prominent problem of CO_2 emissions seriously exceeding the standard [8]. Therefore, it is particularly important to utilize resources efficiently and recycle them. In order to realize this important historical mission, new avenues for geopolymer materials have been opened up [9,10]. Geopolymer, a possible substitute for cement, is a kind of non-crystalline inorganic polymeric material prepared by alkali excitation of silica-aluminate wastes such as fly ash (FA), metakaolin (MK), and blast furnace slag [11,12]. The bonding within the cement hydration products is dominated by van der Waals and hydrogen bonds, whereas the bonding within the geopolymer products is dominated by ionic and covalent bonds, supplemented by van der Waals bonds. Therefore, the geopolymer has higher strength [13–15], better durability [16–18], and high temperature resistance [19,20], and are more environmentally friendly than conventional silicate cements. Liang and Ji [21] found that the red mud-burnt

furnace slag geopolymer mortar (GM) has better corrosion protection for steel reinforcement compared to cement mortar. Shadnia *et al.* [22] studied PCM incorporated GM and found that PCM incorporated GM can reduce cooling and heating energy consumption and increase the thermal inertia of the building effectively. GM is configured by mixing appropriate amount of geopolymer with sand [23], which has higher gel strength than geopolymer, stronger bond than geopolymer concrete, and better corrosion resistance [24], fire resistance, and high temperature resistance [25,26] compared to the ordinary silicate cement mortar, and it is an excellent material for building repair.

With the development of society, the acceleration of the building construction process, as well as the aging of existing building facilities, the performance of building materials put forward new and higher requirements. In previous studies, the pursuit of building materials properties is mainly based on high strength and high toughness, while the problem of structural durability was ignored. However, in the actual engineering, many building structures are damaged before they reach the service life due to the lack of durability for the structures [27]. As a result, the lack of durability caused by the problem of structural damage has always attracted attention. Chen *et al.* [28] explored the durability of hydraulic concrete, and proposed the methods for improving the durability of hydraulic concrete. Wang *et al.* [29] studied the connection between the durability and the corresponding resistance of hydraulic concrete members, and proposed related repair measures to improve the durability. Mansourghanaei *et al.* [30] found that nanoparticles can improve the durability of geopolymer concrete. Therefore, the study of durability of GM is very necessary for the safety of concrete structures.

The use of geopolymers in actual engineering, such as MK-based geopolymers, is still limited due to the disadvantages of relatively high porosity and low interfacial bonding compared with Portland cement. For this reason, scholars have carried out a great deal of research work to enhance related properties of geopolymer composites. The composite reinforcement for blending of fibers and nanomaterials in building materials can effectively enhance the performance of the materials. The commonly used fibers are steel fibers [31–34], basalt fibers [35–37], polypropylene (PP) fibers [38–40], polyvinyl alcohol (PVA) fibers, *etc*. The PVA fibers have a higher modulus of elasticity and abrasion resistance compared to PP fibers, and the adhesive properties are also superior to the steel fibers and basalt fibers. Besides, the PVA fibers exhibit well dispersibility and the cost is lower than that of steel fibers at the same time. Zerfu and Ekaputri [41] explored the performance of concrete containing PVA fibers, and found that geopolymer concrete specimens with and without PVA fibers have better bond strength than ordinary silicate concrete. Jiang *et al.* [42] investigated the formulation and basic mechanical characteristics of high-strength concrete reinforced by PVA fibers and it was found that PVA fibers can improve splitting tensile strength of concrete and enhance the toughness of concrete. At present, it is known that mixing PVA fibers into concrete has improved the compressive strength, abrasion resistance, resistance to freeze–thaw cycle, and impact resistance of concrete to a certain extent.

Besides fibers, nanoparticles have also been used as a reinforcing material to enhance properties of cementitious composites [43]. Nanoparticles with high specific surface area and small particle size have the ability to promote early hydration reaction and fill in the micropores in the matrix. Adding a certain amount of nano-SiO_2 (NS) will reduce the calcium-silicon ratio of concrete, improve the densification, and enhance the adhesion of fibers to the matrix. Kaya [44] investigated that the optimal mixing ratio of NS/Al_2O_3 for the strength of geopolymer paste was 1.60%. Riahi and Nazari [45] studied the compressive strength and abrasion resistance of concrete with NS and CuO, and the specimens with NS were found to have a better increase in abrasion resistance. Zhang and Li [46] found that chloride ion permeability resistance of concrete pavements was enhanced by significant enhancement of nanoparticles. Combining NS with PVA fibers, making full use of the respective advantages of these two materials, and combining the green and environmentally friendly characteristics of GM will bring a broad prospect for the application of GM in civil engineering. Zhang *et al.* [47] investigated the mechanical characteristics of concrete incorporated with PVA fibers and NS, and they found that both NS and PVA fibers could greatly affect the mechanical properties. Malik *et al.* [48] investigated PVA fibers/NS doped geopolymers and discovered that PVA fibers and NS could enhance the structural properties and durability as well as fire resistance of geopolymer composites. Therefore, NS and PVA fibers are able to enhance the durability of GM effectively.

As the machine learning becomes more popular in recent years [49], more and more scholars have predicted and analyzed the material performance and achieved relatively satisfactory results [50–52]. Machine learning can reduce the amount of experimentation and save time by utilizing known datasets to train networks to predict unknown data and structural properties [53]. With a high degree of accuracy, Shao *et al.* [54] predicted the slump, modulus of elasticity, and compressive strength of recycled concrete using a BP neural network (BPNN). Hola and Schabowicz [55]

demonstrated that artificial NNs have good applicability in the evaluation of concrete compressive strength. Tian and Zhu [56] used deep belief network in predicting the durability of concretes with an accuracy of 98%. Huang *et al.* [57] developed a hybrid model of particle swarm optimization (PSO) algorithm and simulated annealing and demonstrated that the algorithm can better predict the strength of rubberized concrete. Jiang *et al.* [58] combined the support vector machines with PSO and predicted the splitting tensile strength of interfaces. Although a lot of experimental research on geopolymer composites and prediction research on concrete composites have been conducted, there is little literature and results can be found on prediction of the durability of geopolymer composites. The PSO-BPNN is applied in this study to predict the durability of GM modified by PVA fiber and NS according to the available experimental results, which can provide a guide for further research on the durability of GM with nanoparticles and PVA fibers.

2 Experiment program

In this study, combined with parameters such as dosage of FA, water reducing admixture, quartz sand, alkali-activator, MK, water, PVA fiber, and NS, particle swarm optimized BP neural network (PSO-BPNN) was utilized to predict and analyze durability of nanoparticles modified GM with PVA fiber. Four material parameters including PVA fiber dosage, NS dosage, MK dosage, and FA dosage which affect the durability of GM were selected as input parameters, and the values of electric flux, loss of compressive strength, and loss of mass of GMs were selected as output values.

The aim of this study is to examine the impact of dosages of NS and PVA fibers on the resistance of chloride ion permeability, freeze–thaw cycles, and sulfate erosion of GMs reinforced with PVA fiber and NS. Therefore, mix proportions were designed using the control variable method, *i.e.*, keeping the dosage and modulus of water glass, water–cement ratio (w/c), and sand ratio unchanged, the dosage of PVA fibers or NS dosage was changed singularly. The water-binder ratio (the ratio of the mass of binding materials to the mass of water in alkali stimulant and additional water) was selected as 0.65, and the ratio of binding material to ratio was 1:1. A comparable quantity of FA was used to replace 30% of the mass of MK. Sodium hydroxide, sodium silicate solution, and water were combined to create the alkali-activator solution in advance. Sodium silicate solution had an initial modulus of 3.2. Flaked sodium hydroxide was added to bring it down to 1.3. Then, water was added to raise the sodium oxide mass fraction to 15% [59]. The NS dosage of 0.5, 1.0, 1.5, 2.0, and 2.5% and PVA fiber volume dosage of 0.2, 0.4, 0.6, 0.8, 1.0, and 1.2% were used for the experiments in this study. Based on their mass ratio, NS was taken in equal proportions of FA and MK.

The main physical properties of the MK are exhibited in Table 1. Besides, the main chemical composition is exhibited in Table 2. The FA used for the experiments had a water absorption of 105%, a bulk density of 0.77 g/cm^3, a standard consistency of 47.1%, and a density of 2.16 g/cm^3. The chemical composition of FA contains 52% SiO_2, 18% Al_2O_3, 6.5% Fe_2O_3, 12.4% CaO + MgO, and 4.3% K_2O + Na_2O. The sodium silicate solution, also known as water glass, had the solid content of 34.3%, and the modulus was adjusted from 3.2 to 1.3 using flake NaOH solids with purity up to 99.0%. The range of particle sizes in the quartz sand was 75–120 μm. PVA fiber measured 40 μm in diameter, 6.5% in elongation and 12 mm in standard length. The tensile strength is 1,560 MPa. The NS was 99.7% pure. The specific surface area is 200 m^2/g, apparent density is 54 g/l, and average particle size is 30 nm. Besides the value of PH is 6.21. Both the cauterization and heating reductions were 1.0%. The pH value of the polycarboxylic acid water reducing agent was 4.52, with the water reduction rate of 21%, and its density was 1.058 g/cm^3.

In this study, different aspects of durability of GM were tested by the sulfate wet and dry cycling test, rapid freeze–thaw cycling test, and electrical flux method, respectively. The resistance to sulfate erosion was measured

Table 2: Main chemical composition of the MK

Chemical constituents	SiO_2	Al_2O_3	Fe_2O_3	CaO + MgO	K_2O + Na_2O
%	54 ± 2	43 ± 2	≤1.3	≤0.8	≤0.7

Table 1: Main physical properties of MK

Lime activity (ml)	Strength activity index (%)	Mean particle size (μm)	Whiteness (%)	Loss on ignition (%)
1,350	12	1.2	70–80	0.5

through tests of sulfate dry-wet cycles. The test was carried out using HC-LSB type automatic dry-wet cycles testing machine for concrete. The mass change rate for the specimen after 90 times dry-wet cycles in the sulfate was determined as the result of assessing the resistance to sulfate erosion of GM. The larger the mass change rate is, the worse the resistance to sulfate erosion of the GM is, and vice versa, the better the resistance to sulfate erosion of the GM. Fast freezing method was used for the freeze–thaw cycles resistance, in which the specimens were subjected to 25 times of rapid freeze–thaw cycle. The compressive strength loss rate after freeze–thaw cycles of the specimen was used to assess the freeze–thaw cycle resistance of GM. The greater the loss rate, the worse the freeze–thaw cycle resistance of the GM, and vice versa, the better the freeze–thaw cycle resistance of the GM. The chloride ion permeability resistance of GM was tested using electric flux method, and the electric flux value was used to assess the chloride ion permeability resistance of GM. The larger the value of electric flux, the worse the chloride ion permeability resistance of GM, and vice versa, the better the chloride ion permeability resistance of GM. The mixing proportions of GMs reinforced by nanoparticles and PVA fiber are shown in Table 3. The related durability indices are shown in Table 4.

Table 4: Durability indices of PVA fiber and NS reinforced GM [60]

Mix no.	Mass loss rate %	Compressive strength loss rate %	Electric flux value C
1	−3.74	18.8	1426.31
2	2.75	17.7	1294.38
3	2.46	15.9	1216.08
4	1.81	14.7	1185.84
5	1.44	12.6	1150.24
6	1.64	10.1	1158.52
7	2.07	8.9	1195.41
8	−2.31	17.1	1220.82
9	−1.12	15.0	1185.06
10	1.6	12.4	1121.13
11	2.1	13.5	1164.84
12	1.9	15.7	1190.52
13	2.06	13.7	1147.62
14	1.47	11.1	1107.48
15	0.82	8.2	1071.78
16	0.99	6.8	1076.94
17	1.38	5.4	1102.36
18	1.67	11.2	1157.88
19	1.21	9.7	1096.02
20	0.92	7.5	1055.16
21	1.15	11.6	1107.06
22	1.49	14.4	1166.98

Table 3: Mixing proportions of NS and PVA fiber reinforced GM [60]

Mix no.	FA kg/m^3	MK kg/m^3	NaOH kg/m^3	Water kg/m^3	Quartz sand kg/m^3	Water glass kg/m^3	NS %	PVA fiber %	Water-reducing agents kg/m^3
1	184.1	429.5	71	106.2	613.6	445.4	0	0	3.07
2	184.1	429.5	71	106.2	613.6	445.4	0	0.2	3.07
3	184.1	429.5	71	106.2	613.6	445.4	0	0.4	3.07
4	184.1	429.5	71	106.2	613.6	445.4	0	0.6	3.07
5	184.1	429.5	71	106.2	613.6	445.4	0	0.8	3.07
6	184.1	429.5	71	106.2	613.6	445.4	0	1.0	3.07
7	184.1	429.5	71	106.2	613.6	445.4	0	1.2	3.07
8	183.1	427.2	71	106.2	613.6	445.4	0.5	0	3.07
9	182.2	425.0	71	106.2	613.6	445.4	1.0	0	3.07
10	181.2	422.7	71	106.2	613.6	445.4	1.5	0	3.07
11	180.2	420.4	71	106.2	613.6	445.4	2.0	0	3.07
12	179.2	418.1	71	106.2	613.6	445.4	2.5	0	3.07
13	182.2	425.0	71	106.2	613.6	445.4	1.0	0.2	3.07
14	182.2	425.0	71	106.2	613.6	445.4	1.0	0.4	3.07
15	182.2	425.0	71	106.2	613.6	445.4	1.0	0.8	3.07
16	182.2	425.0	71	106.2	613.6	445.4	1.0	1.0	3.07
17	182.2	425.0	71	106.2	613.6	445.4	1.0	1.2	3.07
18	183.1	427.2	71	106.2	613.6	445.4	0.5	0.6	3.07
19	182.2	425.0	71	106.2	613.6	445.4	1.0	0.6	3.07
20	181.2	422.7	71	106.2	613.6	445.4	1.5	0.6	3.07
21	180.2	420.4	71	106.2	613.6	445.4	2.0	0.6	3.07
22	179.2	418.1	71	106.2	613.6	445.4	2.5	0.6	3.07

3 Establishment of prediction model

3.1 BPNN

BPNN is a unidirectional propagation of multi-layer feedforward NN, which can be traceable to the 1980s. Three layers make up a typical BPNN. An S-type function serves as the input layer to hidden layer of the transfer function's neurons, and the input and output quantities are from 0 to 1. The essence is to transform a set of input-output problems into nonlinear mapping problems, and through the gradient descent algorithm to solve the weight shot iteratively. The essence is to transform a set of input-output problems into a nonlinear mapping problem, and the weights were iteratively solved through the gradient descent algorithm. The least squares method is the fundamental idea of the BPNN, in which the mean square error (MSE) of the network between the actual and intended output values was minimized by using the gradient search technique.

The learning process is divided into two sections. One section is forward transmission, in which the processing of the hidden layer provides input information through the input layer, and the actual output value can be calculated. The other part is error back propagation, in which the difference between the actual and expected output will be recursively calculated layer by layer if the output layer does not get the expected value, and this difference will be used to adjust the weights and thresholds. To minimize the error signal, these two processes run repeatedly until it reaches the design tolerance within the error range, and then the learning process is over. Figure 1 depicts the BPNN model structure.

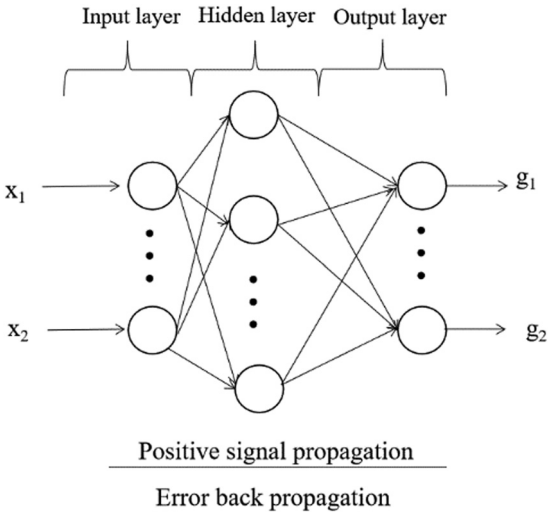

Figure 1: The structure of BPNN.

BPNN can be trained, and it can verify, and predict a large amount of data. The procedures below are involved in setting up a BPNN in MATLAB. At first, the input layer neurons are determined, and then the input data are normalized through the mapminmax function. On this basis of the previous work, the tangent function of S-type tansig serves as the activation function, and the back propagation of learning algorithms is selected as the feedforward algorithm. Subsequently, to build the BPNN, the newff function is called. Then, the maximum number of training cycle steps, learning rate, and learning training minimum error are set. Finally, the sim function is called to have simulation and prediction using the trained model.

3.2 PSO algorithm

Based on an analysis of bird flock feeding behavior, the PSO algorithm was developed, which is also known as bird flock foraging algorithm. PSO algorithm belongs to a kind of evolutionary algorithms, similar to simulated annealing algorithms, starting from a random solution, searching for its best outcome by iteration, and evaluating the quality of the solution through its degree of fitness, which seeks for the global optimum by following the best quality of the current search. The advantages of the PSO algorithm include simplicity and ease of implementation, high accuracy, fast convergence, and no regulation for many parameters. Figure 2 depicts the fundamental steps of the PSO algorithm.

The PSO method is based on the individuals in the swarm sharing information so that a disordered to ordered evolution process is produced in the space of problem solution due to the motion of the whole swarm, and thus the best outcome of the problem can be obtained. When updating the velocity vectors and position vectors of particles, combined with the individual extremes and population extremes of the previous generation, the individual velocities and individual positions can be obtained as follows:

$$V_{\mathrm{id}}^{k+1} = \omega V_{\mathrm{id}}^{k} + c_1 r_1 (P_{\mathrm{id}}^{k} - X_{\mathrm{id}}^{k}) + c_2 r_2 (P_{\mathrm{gd}}^{k} - X_{\mathrm{id}}^{k}), \quad (1)$$

$$X_{\mathrm{id}}^{k+1} = X_{\mathrm{id}}^{k} + V_{\mathrm{id}}^{k+1}, \quad (2)$$

where ω is the inertia weight, r_1 and r_2 are the random numbers from zero to one, c_1 and c_2 are the learning coefficients, V_{id}^{k} is the individual particle velocity for the k-th

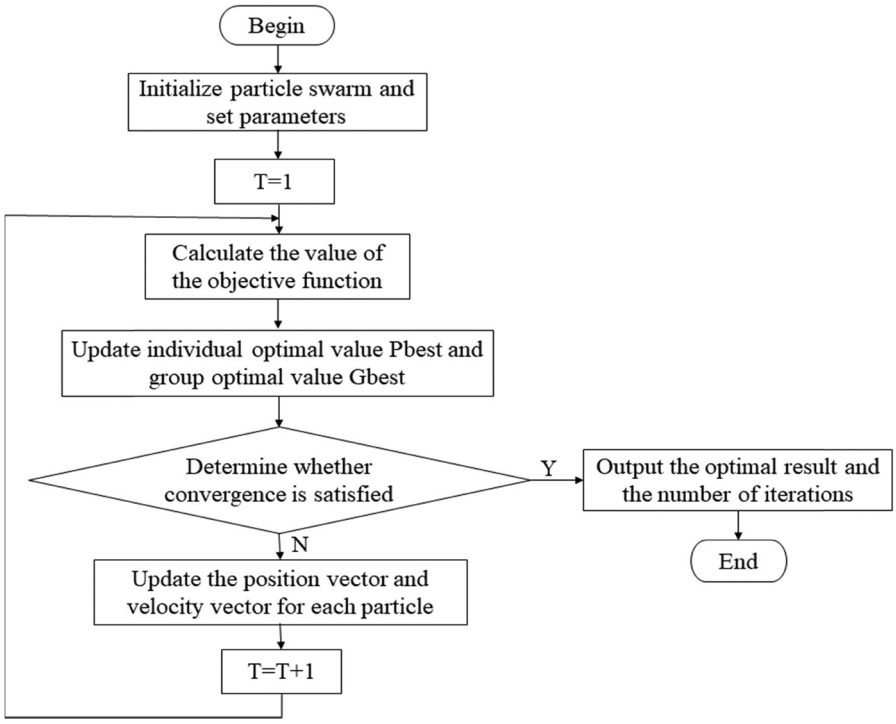

Figure 2: Flow diagram of PSO algorithm.

generation, X_{id}^{k} is the individual particle position for the k-th generation, P_{id}^{k} is the individual particle extreme for the k-th generation, and P_{gd}^{k} is the population extreme of the particles in the k-th generation.

3.3 PSO-BPNN

It has the advantages of simple structure, high accuracy approximation of arbitrary functions, good self-learning ability, and strong nonlinear mapping ability in BPNN. However, this algorithm will show the shortcomings of poor stability, prone to local minima, and slow learning speed when the structure of BPNN is more complex. The PSO algorithm, which carries out learning through population intelligence, has a better global optimization capability. This study combines BPNN and PSO algorithm and proposes a PSO-BPNN model, which produces better computational results, and accelerates the convergence speed of the traditional BPNN algorithm. The steps of PSO-BPNN model establishment are as follows:

(1) Data preprocessing and initialization of the network model parameters.

The training set and test set are separated from the original data. To improve the training speed and sensitivity and simplify the operation, the mapminmax function in MATLAB is used to normalize the data.

For the input and output layers, the quantity of nodes m and n is determined based on the data specifics, and for the implicit layer, equation (3) is used to determine the ideal quantity of nodes l.

$$l = \sqrt{m + n} + \alpha, \tag{3}$$

where α represents the conditioning constant, which is usually taken as an integer.

The initialization PSO parameters can be set as initial population size number, dimension, and the initial position and velocity of each particle is randomly generated within the allowed range. The number of particles, the population size, in the PSO is usually taken as tens to hundreds. The particle dimension D can be defined as the sum of the number of thresholds in implicit and output layer and the number of connection weights between two adjacent layers.

The maximum value of the particle position X_{max} and velocity V_{max} should be set in advance, and the particle position and velocity is initialized randomly within the range of particle position $[-X_{max}, X_{max}]$ and velocity $[-V_{max}, V_{max}]$.

(2) Calculation of the fitness value for every particle.

The fitness value of all particles is initialized to be 0, and then the function is called to calculate the fitness of the particles. The following are the specific steps: a

particle is input first, and then, the mean square deviation of all the samples is calculated, which is the fitness value. Similarly, all the other particles are input until their fitness value is calculated.

(3) Comparing the fitness values to identify the individual and global optimal extreme point for each particle.

If present < P_i, P_i = present, $P_i = X_{id}^k$; otherwise, P_i unchanged,

If present < P_g, P_g = present, $P_g = X_{id}^k$; otherwise, P_g unchanged,

where present denotes the fitness of the current particle. Initialize the best fitness obtained in each iteration, and P_i and P_g denote the individual and global extreme value for particles, respectively.

(4) Determining whether the adaptation value satisfies the preset accuracy.

If the algorithm converges, the thresholds and weights in P_g of the final iteration are mapped to the thresholds and weights of the network. Then, the generalization ability can be verified directly with the test set in the network, otherwise, the next operation will be continued.

(5) Updating the velocity and position of the particles.

The velocity and position of the particles are updated through the formula, and whether they are still within the corresponding limits after the updating will be considered.

Updated location: $X_{id}^{k+1} = X_{id}^k + V_{id}^{k+1}$. If $X_{id}^{k+1} > X_{max}$, then $X_{id}^{k+1} = X_{max}$; if $X_{id}^{k+1} < -X_{max}$, then $X_{id}^{k+1} = -X_{max}$.

Updated speed: $V_{id}^{k+1} = \omega V_{id}^k + c_1 r_1 (P_{id}^k - X_{id}^k) + c_2 r_2 (P_{gd}^k - X_{id}^k)$. If $V_{id}^{k+1} > V_{max}$, then $V_{id}^{k+1} = V_{max}$; if $V_{id}^{k+1} < -V_{max}$, then $V_{id}^{k+1} = -V_{max}$.

(6) Determining whether the iteration can be ended.

Whether the MSE accuracy meets the requirements or whether the number of iterations attains maximum allowed should be determined. The algorithm converges and the thresholds and weights in P_g of the final iteration are mapped to the thresholds and weights of the network when the prediction accuracy is met. Otherwise, the algorithm will be iterated continuously and the operation will be repeated.

(7) Checking the network generalization ability.

The results are input into the test set after the PSO is optimized and BPNN is trained. According to whether the test set adaptation meets the accuracy requirements, the generalization ability is determined. If the adaptability does not meet the accuracy requirements, the preset parameters or the network structure need to be changed to adjust the network, and the above steps are repeated.

(8) Comparing the prediction accuracy.

The prediction accuracy on the test set with PSO-BPNN and unoptimized BPNN is compared, based on which the final conclusion can be drawn.

4 Results analysis and discussion

In this study, the durability of the GM was predicted, using the PSO-BPNN and unoptimized BPNN, respectively. The dosage of water reducer, sodium silicate solution, quartz sand, NaOH, and water were kept constant. The input layer was chosen to include MK dosage, FA dosage, NS dosage, and PVA fibers dosage in the NN, and the values of fluxes were used, while mass loss rate, and compressive strength loss rate were used as the output layers to predict the chlorine ion penetration resistance, freeze–thaw cycle resistance, and sulfate erosion resistance of GM, respectively. The 22 sets of data were divided, 16 sets served as training samples and the rest 6 sets served as test samples for prediction. The NN prediction results were compared with the experimental results to verify the scientificity and rationality of the NNs. Figures 3–5 display the contrast between the predicted and real results for resistance to chloride penetration, freeze–thaw cycle resistance, and sulfate erosion NNs.

According to Figures 3–5, both the NN models have better prediction effect on the GM doped with NS and PVA fiber, but in terms of fitting effect, the PSO-BPNN model is better. Both NS and PVA fibers made a more significant difference on the durability of GM. When the dosage of PVA fibers was constant, the resistance of chlorine ion penetration, freeze–thaw cycle, and sulfate erosion of GM were

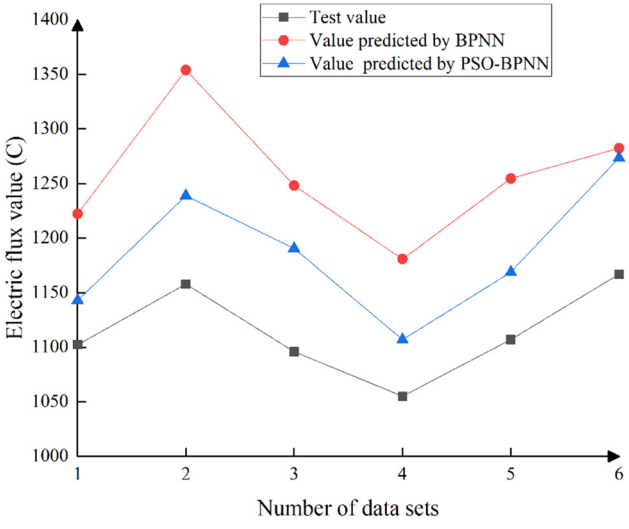

Figure 3: Prediction result of chloride ion permeability resistance of GM.

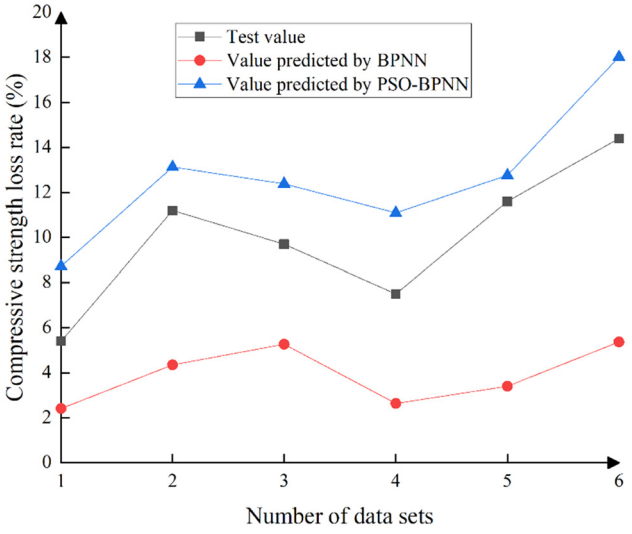

Figure 4: Prediction result of freeze–thaw cycle resistance of GM.

better, *i.e.*, the durability was superior while the dosage of NS was from 1.0 to 2.0% in GM. When the dosage of NS was unchanged and that of PVA fiber was from 0.6 to 1.0%, the durability of GM was better. Besides, when the NS dosage was 1.0% and the PVA fiber dosage was 0.6%, the GM had the best durability. Liu *et al.* [61] found that when the volume fraction of PVA fibers was 0.4%, the mechanical properties and resistance to erosion and wear of the FA based polymer were optimally enhanced, and the resistance to sulfate erosion was improved. Shcherban *et al.* [62] discovered that the optimum PVA fiber dosage in geopolymer composites was 0.6%. While Deng *et al.* [63] found that the optimum dosage of PVA fibers was 0.45 vol% with the highest engineering benefit. Gao *et al.* [64] found that 1.0% of NS resulted in lower porosity and higher strength of geopolymer materials. The above is in agreement with the conclusions of current studies. However, the following studies are not compatible with this study. Li *et al.* [65] reported that FA based geopolymer has the best carbonation resistance when the PVA fiber doping is 2.0%. Bi *et al.* [66] found that the geopolymer containing nano-material has the best performance when the NS content is 0.25%.

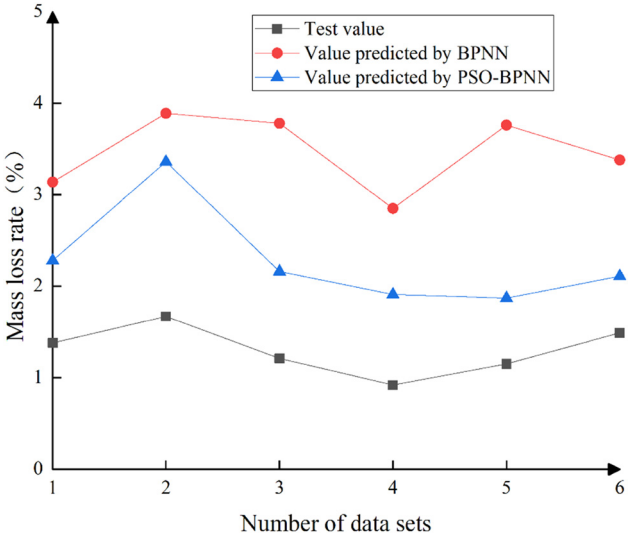

Figure 5: Prediction result of resistance to sulfate attack of GM.

In order to facilitate the comparative analysis and draw the prediction conclusions, this study chooses to analyze the three kinds of errors: MSE, mean absolute value error (MAE), and RMSE, which are calculated using the following formulas:

$$\mathrm{MSE} = \frac{1}{n}\sum_{i=1}^{n}(A_i - F_i)^2, \tag{4}$$

$$\mathrm{MAE} = \frac{1}{n}\sum_{i=1}^{n}|A_i - F_i|, \tag{5}$$

$$\mathrm{RMSE} = \sqrt{\frac{\sum_{i=1}^{n}(A_i - F_i)^2}{n}}, \tag{6}$$

where A_i is the true value, F_i is the value predicted by the model, and n is the number of samples. The error analysis of the prediction of chlorine ion penetration resistance, freeze–thaw cycle resistance, and sulfate erosion resistance of GM by PSO-BPNN and BPNN is exhibited in Tables 5–7.

Table 5: Errors in the prediction of chlorine penetration resistance of GM

NN models	MSE	MAE	RMSE
BPNN	21139.40	142.77	145.39
PSO-BPNN	5826.96	72.67	76.33

Table 6: Errors in the prediction of freeze–thaw cycle resistance of GM

NN models	MSE	MAE	RMSE
BPNN	41.31	6.43	6.06
PSO-BPNN	8.21	2.87	2.72

Table 7: Errors in the prediction of resistance to sulfate attack of GM

NN models	MSE	MAE	RMSE
BPNN	4.79	2.19	2.16
PSO-BPNN	1.06	1.03	0.98

According to Tables 5–7, the durability prediction error of PSO-BPNN for GM is less than that of BPNN. Therefore, PSO-BPNN is feasible for accurate and scientific prediction of the durability performance of GM. This confirms the idea that the PSO-optimized artificial neural network model optimized better in the study by Mashhadban *et al.* [67]. The PSO-BPNN model has higher accuracy and fitting effect in predicting the chlorine ion penetration resistance, freeze–thaw cycle resistance, and sulfate erosion resistance of GM, and it can satisfy the prediction requirements for the loss rate of mass and compressive strength, and the electric flux value, which can provide guidance for the durability study of GM. However, this study has some shortcomings and the study only predicts the durability of GM and should be supplemented with other civil engineering materials as well as other properties to further demonstrate the generalizability of this model. In summary, PSO-BPNN can provide guidance for the durability study of GM blending in PVA fiber and NS, and offer a novel method to predict the performance of GM blending in PVA fiber and NS in the future.

5 Conclusions

1) Strong nonlinear mapping ability and high precision approximation of arbitrary functions are the benefits of the BPNN, but it has low learning speed and poor stability. PSO algorithm has better global optimization ability. PSO-BPNN combines the advantages of the two methods, which can produce better calculation results and speed up the convergence rate of traditional BPNN algorithm.
2) The PSO-BPNN predicts the sulfate erosion resistance, freeze–thaw cycle resistance, and chloride ion permeability of GM with the better fitting effect, smaller errors, and a higher prediction accuracy compared to a single BP neural network.
3) The PSO-BPNN can meet the requirements for the prediction of the loss rate of mass and compressive strength and electric flux value, and can provide guidance for the durability study of GM with PVA fiber and NS, as well as a novel approach to predict the performance of GM blending in NS and PVA fibers in the future.

Funding information: The authors would like to acknowledge the financial support received from National Natural Science Foundation of China (Grant No. 52278283), and Natural Science Foundation of Henan (Grant No. 232300421003).

Author contributions: All authors have accepted responsibility for the entire content of this article and approved its submission.

Conflict of interest: The authors state no conflict of interest.

References

[1] Liu M, Wang CQ, Wu HX, Yang DY, Ma ZM. Reusing recycled powder as eco-friendly binder for sustainable GGBS-based geopolymer considering the effects of recycled powder type and replacement rate. J Clean Prod. 2022;364:132656.
[2] Amran YHM, Alyousef R, Alabduljabbar H, El-Zeadani M. Clean production and properties of geopolymer concrete: A review. J Clean Prod. 2020;251:119679.
[3] Golewski GL, Szostak B. Strength and microstructure of composites with cement matrixes modified by fly ash and active seeds of C-S-H phase. Struct Eng Mech. 2022;82(4):543–56.
[4] Zhang P, Sun XY, Wei JD, Gao Z. Influence of PVA fibers on the durability of cementitious composites under the wet-heat-salt coupling environment. Rev Adv Mater Sci. 2023;62(1):20230115.
[5] Karmokar T, Mohyeddin A, Lee J. Tensile performance of cast-in headed anchors in ambient-temperature cured fly ash-based geopolymer concretes with varying fracture energies. Eng Struct. 2023;282:115827.
[6] Zhang P, Wang C, Guo ZH, Hong J, Wang F. Effect of polyvinyl alcohol fibers on mechanical properties of nano-SiO2-reinforced geopolymer composites under a complex environment. Nanotechnol Rev. 2023;12(1):20230142.
[7] Golewski GL. Assessing of water absorption on concrete composites containing fly ash up to 30% in regards to structures completely immersed in water. Case Stud Constr Mater. 2023;19:e02337.
[8] Zhao J, Wang S, Wang Z, Wang K, Fu C. Bond performance between FRP bars and geopolymer concrete after elevated temperature exposure. Constr Build Mater. 2023;384:131476.
[9] Xu J, Kang A, Wu Z, Xiao P, Gong Y. Evaluation of workability, microstructure and mechanical properties of recycled powder geopolymer reinforced by waste hydrophilic basalt fiber. J Clean Prod. 2023;396:136514.
[10] Shang J, Dai JG, Zhao TJ, Guo SY, Zhang P, Mu B. Alternation of traditional cement mortars using fly ash-based geopolymer mortars modified by slag. J Clean Prod. 2018;203:746–56.
[11] Sadat MR, Muralidharan K, Frantziskonis GN, Zhang LY. From atomic-scale to mesoscale: A characterization of geopolymer composites using molecular dynamics and peridynamics simulations. Comput Mater Sci. 2021;186:110038.
[12] Xu Z, Huang ZP, Liu CJ, Deng H, Deng XW, Hui D, et al. Research progress on key problems of nanomaterials-modified geopolymer concrete. Nanotechnol Rev. 2021;10(1):779–92.
[13] Zhang P, Zhang XM, Zhang YM, Zheng YX, Wang TY. Gray correlation analysis of factors influencing compressive strength and durability of nano-SiO_2 and PVA fiber reinforced geopolymer mortar. Nanotechnol Rev. 2022;11(1):3195–206.

[14] Zhang P, Sun YW, Wu JJ, Hong J, Gao Z. Mechanical properties and microstructure of nano-modified geopolymer concrete containing hybrid fibers after exposure to elevated temperature. Constr Build Mater. 2023;409:134044.
[15] Liu CJ, Huang XC, Wu YY, Deng XW, Liu J, Zheng ZL, et al. Review on the research progress of cement-based and geopolymer materials modified by graphene and graphene oxide. Nanotechnol Rev. 2021;9(1):155–69.
[16] Guo XL, Liu XH, Yuan ST. Effects of initial damage on self-healing of fly ash-based engineered geopolymer composites (FA-EGC). J Build Eng. 2023;74:106901.
[17] Chen KY, Wu DZ, Xia LL, Cai QM, Zhang ZY. Geopolymer concrete durability subjected to aggressive environments - A review of influence factors and comparison with ordinary Portland cement. Constr Build Mater. 2021;279:122496.
[18] Zhang XM, Zhang P, Wang TY, Zheng Y, Qiu LH, Sun SW. Compressive strength and anti-chloride ion penetration assessment of geopolymer mortar merging PVA fiber and nano-SiO_2 using RBF-BP composite neural network. Nanotechnol Rev. 2022;11(1):1181–92.
[19] Giannopoulou I, Robert PM, Sakkas K-M, Petrou MF, Nicolaides D. High temperature performance of geopolymers based on construction and demolition waste. J Build Eng. 2023;72:106575.
[20] Zhang P, Han X, Guo JJ, Hu SW. High-temperature behavior of geopolymer mortar containing nano-silica. Constr Build Mater. 2023;364:129983.
[21] Liang XZ, Ji YS. Experimental study on durability of red mud-blast furnace slag geopolymer mortar. Constr Build Mater. 2021;267:120942.
[22] Shadnia R, Zhang LY, Li PW. Experimental study of geopolymer mortar with incorporated PCM. Constr Build Mater. 2015;84:95–102.
[23] Zhang P, Zheng YX, Wang KJ, Zhang JP. A review on properties of fresh and hardened geopolymer mortar. Compos Pt B-Eng. 2018;152:79–95.
[24] Izzat AM, Al Bakri AMM, Kamarudin H, Moga LM, Ruzaidi GCM, Faheem MTM, et al. Microstructural analysis of geopolymer and ordinary Portland cement mortar exposed to sulfuric acid. Mater Plast. 2013;50(3):171–4.
[25] Zhang P, Han X, Hu SW, Wang J, Wang TY. High-temperature behavior of polyvinyl alcohol fiber-reinforced metakaolin/fly ash-based geopolymer mortar. Compos Part B-Eng. 2022;244:110171.
[26] Ozawa M, Shaikh FUA. A study on spalling behaviour of geopolymer mortars using ring restraint test. Constr Build Mater. 2021;279:122494.
[27] Guo XL, Xiong GY. Resistance of fiber-reinforced fly ash-steel slag based geopolymer mortar to sulfate attack and drying-wetting cycles. Constr Build Mater. 2021;269:121326.
[28] Chen L, Zhang GH, Guan WW, Sun SX. Research on the durability of hydraulic concrete structure. J Water Resour Water Eng. 2006;17(4):62–4.
[29] Wang Y, Zhang HW, Gao R, Wang XD, Yang LQ. Reliability analysis of hydrostructures concrete members. Adv Mater Res. 2013;702:11–4.
[30] Mansourghanaei M, Biklaryan M, Mardookhpour A. Experimental study of the effects of adding silica nanoparticles on the durability of geopolymer concrete. Aust J Civ Eng. 2022;13:2120247.
[31] Zhang P, Wang C, Gao Z, Wang F. A review on fracture properties of steel fiber reinforced concrete. J Build Eng. 2023;67:105975.
[32] Faris MA, Abdullah MMA, Muniandy R, Abu Hashim MF, Bloch K, Jez B, et al. Comparison of hook and straight steel fibers addition on Malaysian fly ash-based geopolymer concrete on the slump, density, water absorption and mechanical properties. Materials. 2021;14(5):1310.
[33] Zhang P, Wang J, Li QF, Wan JY, Ling YF. Mechanical and fracture properties of steel fiber-reinforced geopolymer concrete. Sci Eng Compos Mater. 2021;28(1):299–313.
[34] Rama JSK, Kubair S, Sivakumar MVN, Vasan A, Murthy AR. Fracture properties of ternary blended fiber reinforced self-compacting concrete-A plastic viscosity approach. Comput Concr. 2021;28(4):379–93.
[35] Zheng YX, Zhuo JB, Zhang P, Ma M. Mechanical properties and meso-microscopic mechanism of basalt fiber-reinforced recycled aggregate concrete. J Clean Prod. 2022;370:133555.
[36] Punurai W, Kroehong W, Saptamongkol A, Chindaprasirt P. Mechanical properties, microstructure and drying shrinkage of hybrid fly ash-basalt fiber geopolymer paste. Constr Build Mater. 2018;186:62–70.
[37] Zheng YX, Zhuo JB, Zhang P. A review on durability of nano-SiO_2 and basalt fiber modified recycled aggregate concrete. Constr Build Mater. 2021;304:124659.
[38] Bellum RR. Influence of steel and PP fibers on mechanical and microstructural properties of fly ash-GGBFS based geopolymer composites. Ceram Int. 2022;48(5):6808–18.
[39] Akbar A, Farooq F, Shafique M, Aslam F, Alyousef R, Alabduljabbar H. Sugarcane bagasse ash-based engineered geopolymer mortar incorporating propylene fibers. J Build Eng. 2021;33:101492.
[40] Irshidat MR, Al-Nuaimi N, Rabie M. Thermal behavior and post-heating fracture characteristics of polypropylene microfiber-reinforced geopolymer binders. Constr Build Mater. 2022;332:127310.
[41] Zerfu K, Ekaputri JJ. Bond strength in PVA fibre reinforced fly ash-based geopolymer concrete. Mag Civ Eng. 2021;101(1):10105.
[42] Jiang R, Dong X, Liu X. Research on preparation and elementary mechanical properties of PVA fiber reinforced high-strength concrete. Ind Constr. 2014;44(9):106.
[43] Murthy AR, Ganesh P. Effect of steel fibres and nano silica on fracture properties of medium strength concrete. Adv Concr Constr. 2019;7(3):143–50.
[44] Kaya M. The effect of micro-SiO_2 and micro-Al_2O_3 additive on the strength properties of ceramic powder-based geopolymer pastes. J Mater Cycles Waste. 2022;24(1):333–50.
[45] Riahi S, Nazari A. Compressive strength and abrasion resistance of concrete containing SiO_2 and CuO nanoparticles in different curing media. Sci China-Technol Sci. 2011;54(9):2349–57.
[46] Zhang MH, Li H. The resistance to chloride penetration of concrete containing nano-particles for pavement. Conference on Testing, Reliability, and Application of Micro- and Nano-Material Systems IV: Feb 28-Mar 02 2006. San Diego, CA. Bellingham: Spie-Int Soc Optical Engineering; 2006. p. U161–8.
[47] Zhang P, Fu SD, Zhang KX, Zhang TH. Mechanical properties of polyvinyl alcohol fiber-reinforced concrete composite containing fly ash and nano-SiO_2. Sci Adv Mater. 2018;10(6):769–8.
[48] Malik MA, Sarkar M, Xu SL, Li QH. Effect of PVA/SiO_2 NPs additive on the structural, durability, and fire resistance properties of geopolymers. Appl Sci-Basel. 2019;9(9):1953.
[49] Wang L, Li PY, Zhang W, Wan FY, Wu JX, Yong LQ, et al. Prediction of phase selection of amorphous alloys and high entropy alloys by artificial neural network. Comput Mater Sci. 2023;223:112129.

[50] Lu F, Liang YC, Wang XY, Gao TH, Chen Q, Liu YC, et al. Prediction of amorphous forming ability based on artificial neural network and convolutional neural network. Comput Mater Sci. 2022;210:111464.
[51] Mohammadnejad M, Haghighi-Yazdi M. Prediction of the effective viscoelastic properties of polymer-based microstructure with randomly-placed linear elastic inclusions using convolutional neural network. Compos Mater Sci. 2023;228:112378.
[52] Zhang P, Wang KX, Wang J, Guo JJ, Hu SW, Ling YF. Mechanical properties and prediction of fracture parameters of geopolymer/alkali-activated mortar modified with PVA fiber and nano-SiO_2. Ceram Int. 2020;46(12):20027–37.
[53] Zberecki K. Structure prediction of two-dimensional materials based on neural network-driven evolutionary technique. Comput Mater Sci. 2021;186:110046.
[54] Shao JG, Ji XX, Li R. Application of BP neural network model in the recycled concrete performance prediction. International Conference on Advances in Energy, Environment and Chemical Engineering (AEECE): Sep 26-27 2015. Changsha, Peoples R China. Paris: Atlantis Press; 2015. p. 527–32.
[55] Hola J, Schabowicz K. Application of artificial neural networks to determine concrete compressive strength based on non-destructive tests. J Civ Eng Manage. 2005;11(1):23–32.
[56] Tian X, Zhu NK. Durability prediction method of concrete soil based on deep belief network. Adv Civ Eng. 2022;2022:4338306.
[57] Huang XY, Wu KY, Wang S, Lu T, Lu YF, Deng WC, et al. Compressive strength prediction of rubber concrete based on artificial neural network model with hybrid particle swarm optimization algorithm. Materials. 2022;15(11):3934.
[58] Jiang W, Xie YJ, Li WX, Wu JX, Long GC. Prediction of the splitting tensile strength of the bonding interface by combining the support vector machine with the particle swarm optimization algorithm. Eng Struct. 2021;230:111696.
[59] Sun SW. Adjustment and calculation of water glass modulus. Mine Construct Technol. 1984;1984:26–9.
[60] Wang WC. Study on durability of nano-particles and fiber reinforced geopolymer mortar. Zhengzhou: Zhengzhou University; 2020.
[61] Liu K, Wang Y, Chen C, Ding Z, Shen J. Study on the performance of PVA fiber reinforced fly ash-based geopolymer. Non-metallic Mines. 2021;44(6):94.
[62] Shcherban EM, Beskopylny AN, Stel'makh SA, Mailyan LR, Meskhi B, Shilov AA, et al. Combined effect of ceramic waste powder additives and PVA on the structure and properties of geopolymer concrete used for finishing facades of buildings. Materials. 2023;16(8):3259.
[63] Deng ZM, Yang ZF, Bian J, Pan XX, Wu GL, Guo F, et al. Engineering properties of PVA fibre-reinforced geopolymer mortar containing waste oyster shells. Materials. 2022;15(19):7013.
[64] Gao K, Lin KL, Wang DY, Shiu HS, Hwang CL, Tuan BLA, et al. Thin-film-transistor liquid-crystal display waste glass and nano-SiO_2 as substitute sources for metakaolin-based geopolymer. Environ Prog Sustain Energy. 2014;33(3):947–55.
[65] Li FP, Chen DF, Yang ZM, Lu YY, Zhang HJ, Li S. Effect of mixed fibers on fly ash-based geopolymer resistance against carbonation. Constr Build Mater. 2022;322:126394.
[66] Bi SG, Liu M, Shen JJ, Hu XM, Zhang LY. Ultrahigh self-sensing performance of geopolymer nanocomposites via unique interface engineering. ACS Appl Mater Interfaces. 2017;9(14):12851–8.
[67] Mashhadban H, Kutanaei HH, Sayarinejad MA. Prediction and modeling of mechanical properties in fiber reinforced self-compacting concrete using particle swarm optimization algorithm and artificial neural network. Constr Build Mater. 2016;119:277–87.